23 Why is it Worth Flying at Dusk for Aquatic Insects? Polarotactic Water Detection is most Efficient at Low Solar Elevations

It is a well-documented phenomenon that aquatic insects, especially the small-bodied ones, seek for new habitats during their migration and dispersal generally at dusk (e.g. Popham 1964; Danilevskii 1965; Johnson 1969; Fernando and Galbraith 1973; Zalom et al. 1979, 1980; Saunders 1981; Danthanarayana 1986). From an ecological point of view this is explained conventionally by the reduced risk of both predation and dehydration as well as by the period of calm and optimal air temperature at twilight (e.g. Landin 1968; Landin and Stark 1973). At sunset the intensity of ambient light decreases rapidly with time rendering more difficult the visual detection of flying preys by birds (e.g. King and Wrubleski 1998). Furthermore, at nightfall the lower temperature, higher humidity and calmness of air relative to those in daytime are optimal for small-bodied aquatic insects (Landin and Stark 1973), which can be drifted away by wind and can easily become dehydrated during flight if they cannot find a water body within about one hour.

Bernáth et al. (2003) showed that a further visual ecological factor could also play an important role in the preference of twilight period for habitat finding by polarotactic water insects detecting water by means of the horizontally polarized light reflected from the water surface (Schwind 1991, 1995). They presented experimental and computational evidence for the phenomenon that polarotactic water detection is most efficient at low solar elevations. To prove this, the reflection-polarizational characteristics of the full surface of water bodies of different optical types should be measured and compared as a function of the solar elevation. Although imaging polarimetric measurements of these characteristics have been performed previously (e.g. Horváth and Zeil 1996; Horváth and Varjú 1997; Horváth et al. 1997, 1998a; Kriska et al. 1998; Bernáth et al. 2002), they were restricted to relatively small (maximum about $40^o \times 50^o$) fields of view. The method of 180^o field-of-view imaging polarimetry developed by Gál et al. (2001b,c) and Horváth et al. (2002a) made it possible to measure the reflection-polarization patterns of the whole water surface in a hemispherical field of view, the half aperture of which ranges from the nadir to the horizon.

Since the down-facing polarimeter must be suspended somehow above the water surface which must not undulate during recording, it is enormously difficult to perform such comparative measurements above real water surfaces versus time. The requirement of cloudless sky and completely windless weather ensuring flat

water surfaces without ripples throughout the day makes comparative polarimetric measurements almost impossible. Thus, Bernáth et al. (2003) decided to use water-imitating artificial surfaces, called "water-dummies". These dummies were composed of a horizontal glass pane underlain by either a black or a grey substratum in order to eliminate the inevitable rippling of natural water surfaces. Such reflecting surfaces with manipulated reflection-polarizational and spectral characteristics were successfully applied by Schwind (1991, 1995) to study the polarotaxis of water insects. Bernáth et al. (2003) compared the reflection-polarization patterns of both water-dummies measured in the red (650 nm), green (550 nm) and blue (450 nm) spectral ranges under clear skies from sunrise to sunset as a function of the solar elevation.

Bernáth et al. (2003) calculated the percentage Q of the lower hemispherical visual field, in which the two water-dummies are considered as water by a hypothetical polarotactic water insect versus the solar elevation θ_S. The reflection-polarization patterns and the derived Q-values were also calculated as a function of θ_S for a perfectly black horizontal reflector absorbing all penetrating light for both indices of refraction n_w=1.33 and n_g=1.5 of water and glass, respectively. Bernáth et al. (2003) showed that the difference between the Q-values calculated for water and glass are smaller than 4%, which is practically negligible. Thus the conclusions drawn from the data obtained for the glass water-dummies also hold for flat water surfaces.

23.1. Measurement and Computation of the Reflection-Polarizational Characteristics of the Water Dummies

One of the two water-dummies of Bernáth et al. (2003) was composed of a horizontal glass pane (1m × 1m) underlain by a ply-wood covered with a matt black cloth. This imitated dark water bodies with transparent water and black bottom, or deep waters, from the subsurface layers of which only small amount of light is returned. The other water-dummy was a horizontal glass pane (1m × 1m) underlain with a ply-wood covered by a matt light grey cloth. It mimicked bright waters with transparent shallow water and bright bottom, or waters with bright suspended particles, from which considerable amount of light is returned in comparison with the amount of surface-reflected light. The relative reflectivity of the black and grey cloths (Fig. 23.1A) and the water dummies (Fig. 23.1B) versus the wavelength was measured with a Jobin Yvon-Spex Fluoromax-2 spectrofluorimeter. The water-dummies were laid horizontally on levelled metal holders 30 cm above the ground (Fig. 23.2A) on a hill top in order to minimise the disturbing mirroring of landmarks near the horizon. The horizontality of the dummies was checked by water levels.

Bernáth et al. (2003) used the 180° field-of-view imaging polarimeter described by Gál et al. (2001b,c). The polarimeter with down-facing fisheye lens was suspended on a holder above the centre of the water-dummy in such a way, that the vertical optical axis of the lens pointed towards the nadir (Fig. 23.2A). In order

to minimise the disturbance of the shadow of the holder on the dummy surface, different holder orientations relative to magnetic north were chosen as shown in Figs. 23.2B and 23.2C. The distance between the outermost surface of the fisheye lens and the glass surface was as small as possible (7 cm) in order to measure the reflection-polarizational characteristics of the water-dummies in a conical field of view as wide as possible (about 160^o). The fisheye lens was focused into infinity to record the mirror image of the sky reflected from the glass surface. For a complete measurement three photographs were taken through the polarizers with three different transmission axes. This needed about 10 seconds, during which the operator triggered the expositions by a remote cord and turned the filter wheel of the polarimeter three-times. During measurements the operator lay on the ground below the level of the glass pane to avoid unwanted reflections (Fig. 23.2A). After the measurement of the reflection-polarization pattern of a water-dummy, the dummy was replaced by the other one within about 1 minute and the procedure was repeated. This allowed to measure the reflection-polarization patterns of both dummies within about a few minutes, that is, practically under the same illumination conditions and at the same solar elevation θ_S.

Measurements were carried out near the time of the summer solstice under sunny, partly cloudy skies on 17 July 2002 and on 18 July 2002 under sunny, cloudless clear skies near Kunfehértó in Hungary (46°23'N, 19°24'E) from sunrise (4:49, local summer time = UTC+2) to sunset (20:37) at different θ_S shown in Figs. 23.2B and 23.2C, respectively. The maximum of θ_S was 67° at noon (12:56). Because of disturbing early morning dewfall, reflection-polarization patterns at low solar elevations are presented here only for the sunset and dusk period.

Although during measurements the direction of the polarimeter holder relative to the fixed dummies below the polarimeter changed and the sun moved along its celestial arc (Figs. 23.2B and 23.2C), for the sake of a better visualization in Figs. 23.3-23.5 we present all circular pictures rotated in such a way, that the actual solar meridian points always vertically upward, since these patterns are symmetrical to the solar-antisolar meridian under clear skies.

The mirror image of the polarimeter, its holder and the remote cord as well as their shadows (Fig. 23.2A) moved counter-clockwise with respect to the solar meridian versus time (Figs. 23.3 and 23.4). Since the major aim was to compare the reflection-polarization patterns of the two water-dummies and the numerical values of a derived quantity Q, from comparative analysis the regions (chequered in Figs. 23.3 and 23.4) were excluded, in which landscape near the horizon, or unwanted overexposure, or disturbing shadows and mirror images of the polarimeter, its holder and remote cord occurred in the individual pictures taken at a given θ_S. Thus for both dummies at a particular θ_S a mask was obtained, the area of which was inappropriate for comparative analysis: directions of view within the time-dependent mask were not taken into account. Hence, in comparative analysis only those viewing directions were considered, where the mirror image of the sky and the polarizational characteristics of reflected skylight could be registered without any disturbance.

The reflection-polarization patterns of a perfectly black water-dummy, absorbing the penetrating component of incident light, shown in Fig. 23.5 were calculated with the mathematical method developed by Schwind and Horváth (1993), Horváth (1995a) and Gál et al. (2001b) for incident single-scattered Rayleigh skylight.

23.2. Calculation of the Area of the Water Dummies in which they are Considered as Water by a Hypothetical Polarotactic Insect

Schwind (1985b) showed that backswimmers (*Notonecta glauca*) avoid a light source emitting vertically polarized light. The same was demonstrated in dragonflies (Horváth et al. 1998a; Wildermuth 1998), mayflies and many other water-loving insects (Schwind 1991, 1995; Kriska et al. 1998; Bernáth et al. 2001b). Thus, it is logical to assume, that polarotactic water insects consider any surface as water, if the degree of linear polarization p of reflected light is higher than the threshold p_{tr} of polarization sensitivity and the deviation $\Delta\alpha$ of the angle of polarization of reflected light from the horizontal is smaller than a threshold $\Delta\alpha_{tr}$ in that part of the spectrum in which the polarization of reflected light is perceived. An imaginary polarotactic water insect levitating above the center of the water-dummies was assumed to take those areas of the dummies for water from which skylight is reflected with the following two characteristics: $p > p_{tr}$ and $|\alpha–90^{o}| < \Delta\alpha_{tr}$. The "percentage Q detected as water" was introduced, which is the angular proportion Q of the viewing directions for which both criteria are satisfied relative to the angular extension of 2π steradians of the whole lower hemisphere of the field of view of the insect. In other words, Q gives the relative proportion of the entire ventral field of view in which the water-dummies are considered polarotactically as water. The percentages Q detected as water calculated for the grey water-dummy were compared with those of the black dummy in the blue (450 nm), green (550 nm) and red (650 nm) parts of the spectrum.

23.3. The Reflection-Polarization Patterns of the Water Dummies

Column 1 in Figs. 23.3 and 23.4 shows the colour photographs (without polarizers) of the mirror image of the clear sky reflected from the grey and black water-dummies, respectively, as a function of the solar elevation θ_S. We can see the unavoidable disturbing mirror images of the fisheye lens of the polarimeter, its holder and remote cord as well as their inevitable shadows opposite to the mirror image of the sun. Several photographs are overexposed in the vicinity of the mirror sun and in some cases also near the horizon due to the great amount of light

reflected from the glass surface. In some cases also a bright spot occurs opposite to the mirror sun due to the internal reflection of sunlight from the refractive surfaces of the fisheye optics composed of several individual lenses. Although the water-dummies fill the major part of the field of view of the polarimeter due to its small distance from the glass surface, at the periphery of the pictures the landscape is seen near the horizon. All areas of the pictures with these unwanted disturbances (chequered in Figs. 23.3 and 23.4) were recognized during the computer evaluation and they were considered as regions inappropriate for comparative analysis. Since these colour photographs were taken with different times of exposure, they do not display correctly the relative intensity of reflected light. They serve only for demonstration of the mirror images of the clear skies, under which the reflection-polarization patterns of the water-dummies were recorded. Nevertheless, it is clear from these photographs, that the amount of light reflected from the glass surface dominates relative to the cloth-reflected amount of light in the case of the black water-dummy (Fig. 23.4), while at the grey dummy (Fig. 23.3) the latter component also contributes significantly to the net amount of returned light.

Column 2 in Figs. 23.3 and 23.4 shows the patterns of the degree of linear polarization p of skylight reflected from the grey and black water-dummies in the blue (450 nm) versus θ_S. Comparing the p-patterns of the two dummies, we see that the grey water-dummy is less polarizing than the black one. The light reflected from the grey dummy is almost unpolarized in many directions of view, and its maximum p is only about 30%. At the Brewster angle (56° from the nadir for glass) very low p-values occur in many azimuth angles. On the other hand, the black water-dummy is an effective polarizer reflecting highly polarized skylight from many directions of view. At the Brewster angle a continuous annular zone occurs with maximum p. Depending on θ_S, two neutral points with unpolarized reflected skylight appear within the Brewster zone perpendicularly to the solar meridian.

Column 3 in Figs. 23.3 and 23.4 shows the patterns of the angle of polarization α of skylight reflected from the water-dummies in the blue (450 nm) as a function of θ_S. There are again considerable differences in the α-patterns between the two water-dummies. At the grey dummy as θ_S increases the proportion of the nearly vertically polarized reflected skylight with $-45^o < \alpha < +45^o$ shaded by red and yellow becomes dominant over the nearly horizontally polarized reflected skylight with $45^o < \alpha < 135^o$ shaded by green and blue, especially perpendicularly to the solar meridian. However, from regions of the grey water-dummy toward the mirror sun always approximately horizontally polarized light is reflected. At near-zero solar elevations this is the case also for regions toward the mirror antisun. From the Brewster zone of the grey dummy always nearly vertically polarized light is reflected perpendicularly to the solar meridian. From the black water-dummy always predominatly nearly horizontally polarized skylight is reflected irrespectively of θ_S. However, approximately vertically polarized skylight is reflected from 8-shaped regions with long axes perpendicular to the solar-antisolar meridian within the Brewster zone as well as from crescent-shaped areas near the

horizon perpendicularly to the solar meridian. From the Brewster zone of the black dummy always horizontally polarized skylight is reflected. Note that the mirror images of the polarimeter, its holder and remote cord disturb the α-patterns only slightly. Therefore in these regions we omitted the chequered pattern in the α-maps of Figs. 23.3 and 23.4. These regions were, however, not taken into account in comparative analysis.

23.4. Areas of the Dummies Detected as Water

In column 4 of Figs. 23.3 and 23.4, the regions of the water-dummies are shaded by black, where $p > p_{tr} = 5\%$ and $|\alpha - 90^o| < \Delta\alpha_{tr} = 5^o$, assuming that the imaginary polarotactic insect detects the water in the blue (450 nm). Analysing these patterns, we can see that at $\theta_S \approx 0^o$ the grey water-dummy is taken for water only in areas towards the mirror sun and mirror antisun and partly in the Brewster zone. As θ_S increases, the area detected as water gradually decreases and the grey dummy is considered as water only in small spots around the mirror sun and opposite to it. At higher θ_S the grey dummy is not taken as water in the Brewster zone. On the other hand, the black water-dummy is always considered as water at and near the Brewster angle. Farther away from the Brewster angle the black dummy is not taken for water perpendicularly to the solar meridian. Since in the green (550 nm) and red (650 nm) quite similar patterns were obtained as those in Figs. 23.3 and 23.4, we omit to present them.

Figure 23.5 shows the p- and α-patterns and the areas detected as water of a perfectly black glass (index of refraction $n_g = 1.5$) reflector absorbing all penetrating light computed for the same θ_S as in Figs. 23.3 and 23.4 and for incident single-scattered Rayleigh skylight. We can see that the patterns in Fig. 23.5 are very similar to those in Fig. 23.4, hence the reflection-polarizational characteristics of the black water dummy approximate those of a perfectly black glass reflector. The same patterns were also computed for a perfectly black water reflector with an index of refraction $n_w = 1.33$, and practically the same results were obtained. Hence the slightly higher index of refraction of glass makes the reflection-polarizational characteristics of glass surfaces only a little different from those of water: p of light reflected from the glass is slightly higher and the Brewster angle $\theta_B = 56°$ of glass is slightly larger than that of the water ($\theta_B = 53°$), for example. Thus the conclusions drawn from the data obtained for the glass water-dummies also hold for flat water surfaces.

Since in the literature there are no reliable data about the thresholds p_{tr} and $\Delta\alpha_{tr}$ of polarization sensitivity in any water insect, one has to set their numerical values arbitrarily. To study how the percentage Q detected as water depends on these thresholds, Q was calculated as functions of them for both water-dummies. The results are shown in Fig. 23.6 in the intervals $0\% < p_{tr} < 10\%$ and $0^o < |\Delta\alpha_{tr}| < 10^o$ for the blue (450 nm) spectral range. Since the $Q(d_{tr})$ and $Q(\Delta\alpha_{tr})$ curves continued similarly outside these intervals and very similar curves were obtained

for both the green (550 nm) and red (650 nm) spectral ranges, we omit to display these curves outside these intervals and in other parts of the spectrum. It is clear from Fig. 23.6 that increasing the threshold p_{tr}, Q decreases monotonously, and the increase of threshold $\Delta\alpha_{tr}$ results in the monotonous increase of Q. Since there are no sudden changes, or local extrema, or breaking points, or plateaus, for instance, in the $Q(p_{tr})$ and $Q(\Delta\alpha_{tr})$ curves, one could not establish any criterion for a threshold value which could be preferred. This fact has the important consequence, that the values of these two thresholds can indeed be chosen arbitrarily, and the actual choice concerns neither the relative values of Q calculated for different θ_S nor the conclusions drawn from them. Selecting other values of p_{tr} and $\Delta\alpha_{tr}$ would change only the absolute Q-values but not the qualitative shape of the $Q(p_{tr})$ and $Q(\Delta\alpha_{tr})$ curves versus θ_S. Thus the arbitrary use of $p_{tr} = 5\%$ and $|\Delta\alpha_{tr}| = 5°$ is not a serious restriction.

The left column in Figs. 23.7 and 23.8 shows the percentage Q detected as water calculated for the grey and black water-dummies under a clear and a partly cloudy sky as well as for the perfectly black glass ($n_g = 1.5$) and water ($n_w = 1.33$) reflectors as a function of θ_S in the blue (450 nm), green (550 nm) and red (650 nm). The $Q(\theta_S)$ curves of the perfectly black reflectors are approximately the same in all three spectral ranges, since the slight wavelength-dependency of the refractive indices of glass and water can be neglected in the visible part of the spectrum. The $Q(\theta_S)$ curves of the perfectly black reflectors were calculated for the full surface of the reflectors (dashed curves) as well as for the masked surface, that is, for regions appropriate for comparative analysis (individual data points displayed with triangles). The right column in Figs. 23.7 and 23.8 shows the difference ΔQ between the grey and black water-dummies as well as between the perfectly black glass and water reflectors. In Figs. 23.7 and 23.8 the following are seen:

- The differences ΔQ between the perfectly black glass and water reflectors are smaller than a few percents, the maximum difference is $\Delta Q_{max} = 4\%$ for $\theta_S \approx 0^o$ and $\Delta Q = 2\%$ for higher θ_S. This also shows that the conclusions drawn from the data obtained with the glass water-dummies can be extended also to flat water surfaces.
- The differences ΔQ between the full and masked surfaces of the perfectly black reflectors are smaller than 5%. From this one can conclude that the use of the masks (e.g. chequered in Figs. 23.3 and 23.4) in comparative analysis does not change significantly the Q-values calculated for different θ_S and for the two water-dummies. In other words, disregarding from the regions being inappropriate for comparative analysis does not concern the conclusions drawn from the remaining parts of the measured reflection-polarization patterns of the water-dummies.
- At $\theta_S \approx 0^o$ the percentage Q detected as water is maximal for the grey water-dummy and has a local maximum for the black dummy in all three spectral ranges. Thus in the visible part of the spectrum, polarotactic detection of brighter water bodies is most efficient when the sun is approximately at the

horizon. The $Q(\theta_S)$ curve of the black water-dummy has a local minimum at $\theta_S \approx 30^o$ in all three spectral ranges. For higher solar elevations $Q(\theta_S)$ of the black dummy is as high as or even higher than that at $\theta_S \approx 0^o$. Thus in the visible part of the spectrum, polarotactic detection of dark water bodies is most efficient when the sun is either approximately at the horizon or near the zenith.

- The difference ΔQ between the grey and black water-dummies is minimal at low solar elevations in all three parts of the spectrum.

For both water-dummies, more than 85% of the region appropriate for comparative analysis satisfies the degree of polarization criterion $p > p_{tr} = 5\%$. Q of the grey water-dummy is significantly smaller than that of the black dummy. However, according to the angle of polarization criterion $|\alpha–90^o| < \Delta\alpha_{tr} = 5^o$ alone, maximum 40% of the region appropriate for comparative analysis is detected as water for both water-dummies, and Q of the grey dummy is significantly smaller again than that of the black dummy. Since in any direction of view the α-criterion is always satisfied if the p-criterion is satisfied, polarotatic water detection is limited by the α-criterion in the case of the used thresholds $p_{tr} = 5\%$ and $\Delta\alpha_{tr} = 5^o$.

23.5. Discussion

The reflection-polarizational characteristics of water surfaces depend on the illumination conditions, material composition of the bottom, dissolved organic materials, angle of view measured from the nadir and the direction of observation relative to the sun. Aquatic insects can identify their water habitat by perceiving the partial linear polarization of light reflected from the water surface if the degree of linear polarization is high enough and the direction of polarization approximates the horizontal. These two criteria are satisfied predominantly in the Brewster zone, which is continuous throughout the day at dark water bodies, but for bright waters this is true only towards the sun and antisun and in the time of sunrise and sunset. During the day the percentage Q detected as water is such low at bright water bodies, that they can be easily overlooked by water insects. In the case of bright water surfaces the shape and direction of the regions suitable for polarotactic water detection change considerably with the changing solar elevation (column 4 in Figs. 23.3 and 23.4). Therefore bright aquatic habitats can be recognised polarotactically only from certain directions of view with respect to the sun.

If the polarization of light reflected from water is analyzed in the whole lower hemisphere of the visual field of a flying and water-seeking imaginary polarotactic insect, the percentage Q detected as water is proportional to the chance a water body is recognized as water in the optical environment. Then in the visible part of the spectrum, polarotactic water detection is most efficient in the sunrise and sunset periods, when Q is maximal, the reflection-polarizational characteristics of dark and bright waters are most similar and the risk of escaping the attention of polarotactic water-seeking insects is minimal. This conclusion is valid also for a

visual field of the ventral polarization-sensitive eye region which is much narrower than the whole lower hemisphere, because the areas detected as water are centred at or near the Brewster angle (see column 4 of Figs. 23.3, 23.4 and column 3 of Fig. 23.5).

In field experiments, in which huge white and black shiny plastic sheets were laid onto the ground in summer as water dummies Bernáth et al. (2001a,b) observed that during daytime only large- or medium-bodied (1-5 cm) aquatic insects (e.g. *Dytiscidae, Hydrophilidae, Notonectidae*) were attracted to the black plastic sheet. These beetles can fly for a few hours also daytime at higher temperature and lower humidity of the air due to their larger size with a smaller surface/volume ratio and to their thick sclerotized cuticle, which slows down the dangerous dehydration of the body. Small-bodied water bugs (1-5 mm, e.g. *Sigara* sp.) were lured to the black plastic sheet *en masse* exclusively at and after sunset. These insects possess such a large surface/volume ratio and thin chitinuous cuticle, that they can become easily dehydrated during flight of a few tens minutes. Their flight can also be hindered by wind, which usually abates at sunset when direct solar radiation quickly decreases to zero (Landin and Stark 1973). The sunrise period is less optimal for dispersal of aquatic insects than the sunset period, because at dawn the air temperature is much lower than at dusk (Landin 1968; Landin and Stark 1973). This may be one of the reasons why small-bodied aquatic insects generally migrate *en masse* in the sunset and dusk period.

However, the medium-bodied backswimmer *Notonecta glauca* seems to be an exception from this rule. Apart from *Notonecta glauca*, the angular extension of the ventral eye region, in which the polarization of light reflected from water is analyzed, is unknown in aquatic insects. In *Notonecta* the ventral eye region, in which the microvilli of the UV-sensitive central photoreceptors R7 and R8 are orthogonal, extends up to a nadir angle of about 35^o (Schwind 1983b). This eye region is optimal for the analysis of the horizontal polarization of water-reflected light. According to Schwind (1983b, 1985b), in *Notonecta* the reflection polarization of water surfaces may be analyzed by an approximately 3^o wide narrow annular zone ranging from nadir angles 32^o to 35^o. Figure 23.9 shows the $Q(\theta_S)$ curves of the perfectly black water and glass reflectors in the red, green and blue spectral ranges calculated for the circular region with nadir angle 35^o and for the annular region between nadir angles 32^o and 35^o (see also column 3 in Fig. 23.5). Similar calculations cannot be performed for the measured patterns of the black and grey water-dummies, because around the nadir they are not appropriate for evaluation due to the mirror image and the shadow of the polarimeter (see the central chequered areas in the circular patterns of Figs. 23.3 and 23.4). From Fig. 23.9 we can see that in the case of the regions around the nadir, corresponding with the field of view of the mentioned ventral circular and annular eye regions in *Notonecta*, Q increases with increasing θ_S. Hence, for *Notonecta* the polarotactic detection of dark waters is most efficient for higher solar elevations. This could be the reason why Bernáth et al. (2001b) observed frequently the landing of *Notonecta* on the black plastic sheet during the day rather than at dusk.

Bernáth et al. (2003) used p_{tr} = 5% as the p-threshold of the imaginary polarotactic insect. The threshold of the highly polarization-sensitive

monochromatic photoreceptors in the specialized dorsal rim area of the compound eye in the honeybee *Apis mellifera* is about p_{tr} = 10% and in the field cricket *Gryllus campestris* p_{tr} = 5% (Labhart 1980; Labhart et al. 1984). In insects associated with water the value of this threshold is completely unknown, and it could be species-specific. When Schwind (1995) determined the spectral regions in which some aquatic insect species perceive the polarization of reflected light, he assumed rather arbitrarily a threshold p_{tr} = 35%. However, he has also emphasized that the assumed threshold value did not crucially affect his conclusions.

Under clear skies at a given θ_S the reflection-polarizational characteristics of the water-dummies as well as real water bodies depend on two components of returned light: (1) The first component is the light reflected from the glass/water surface. The direction of polarization (E-vector direction) of this partially polarized component is always horizontal except in small regions within the Brewster zone, and if the angle of reflection is equal to the Brewster angle, it is totally polarized (p = 100%). (2) The second component is the light originating from below the surface due to reflection from the underlying substratum or from the bottom of water, or to backscattering from particles suspended in water. This component is always vertically polarized due to refraction at the surface (Horváth and Pomozi 1997). The net degree and direction of polarization of the returned light are determined by the polarizational features and relative intensities of these two components. Since these two components have orthogonal directions of polarization, their superposition reduces the net p. If the intensity of the first component is greater than that of the second one, the returned light is partially linearly polarized with horizontal E-vector. When the second component is the more intense, the returned light is partially vertically polarized. Finally, if the intensities of these two components are approximately equal, the returned light is nearly unpolarized.

In the case of a perfectly black reflector only the surface-reflected first component exists. The resulting reflection-polarization patterns under clear skies versus θ_S are shown in Fig. 23.5, where the following trend is seen: the lower the θ_S, the smaller is the proportion of the nearly horizontally polarized ($45^o < \alpha < 135^o$) reflected skylight. Since the percentage Q detected as water is determined predominantly by α of reflected skylight, the same trend occurs for the change of Q versus θ_S: the lower the θ_S, the smaller is Q, as seen in the left column of Figs. 23.7 and 23.8. The $Q(\theta_S)$ curve has a flat local maximum at $\theta_S = 5^o$, due to the interference of the θ_S-dependent complex p- and α-patterns in the determination of the value of Q. Q is maximal (about 96%) when the sun is at the zenith. Although then both the incident and reflected skylight are horizontally polarized, regions of the surface within and outside the Brewster zone reflect light with almost zero degrees of polarization, and due to the criterion $p > p_{tr}$ = 5% for successful water detection, Q cannot be as high as 100%.

Although in the case of the black water-dummy also the subsurface-reflected second component exists, the reflection-polarizational characteristics and the shape of the $Q(\theta_S)$ curve are similar to those of the perfectly black reflector, since

the intensity of the second component is small relative to that of the surface-reflected first component. The major difference is that the skylight reflected from the black water-dummy is less polarized (column 2 in Fig. 23.4) than the skylight reflected from the perfectly black reflector (column 1 in Fig. 23.5) due to the depolarising effect of the second component. This lower p is the reason for the lower Q of the black water-dummy relative to that of the perfectly black reflector (left column in Figs. 23.7 and 23.8).

For the grey water-dummy the vertically polarized second component from the subsurface is such intense that it depolarises considerably the horizontally polarized surface-reflected first component (column 2 in Fig. 23.3). At lower θ_S the first component is the more intense towards the mirror sun and mirror antisun resulting in nearly horizontally polarized reflected light, while perpendicularly to the solar-antisolar meridian the second component is the more intense causing nearly vertically polarized reflected light (column 3 in Fig. 23.3). As θ_S increases, the relative intensity of the second component increases, thus the proportion of the nearly horizontally polarized reflected light decreases, resulting in the decrease of the percentage Q detected as water (column 4 in Fig. 23.3). For $\theta_S > 20^o$ the amount of subsurface-reflected light is such enhanced that Q becomes smaller than 10% (left column in Figs. 23.7 and 23.8).

The polarimetric technique of Bernáth et al. (2003) used a fisheye lens including numerous optical elements made of ultraviolet-absorbing glasses. For polarimetric measurements in the ultraviolet (UV) spectral range, a UV-transmitting fisheye lens composed of quartz would be needed, but such an objective is not available in the market. In the UV, the second component of returned light originating from below the water surface is considerably reduced in natural water bodies due to the great absorption by the dissolved organic materials and to the low reflectivity of the bottom (Schwind 1995; Bernáth et al. 2002). Thus in the UV, the majority of natural water bodies has similar reflection-polarizational characteristics and $Q(\theta_S)$ curve as the black water-dummy has in the blue (Figs. 23.4, 23.7 and 23.8). Consequently, although Bernáth et al. (2003) could not measure the reflection-polarization patterns of the water-dummies in the UV, the conclusions hold also for this part of the spectrum.

Comparing Figs. 23.7 and 23.8, we can establish that the $Q(\theta_S)$ curves of the water-dummies possess the same qualitative features under clear and partly cloudy skies. The light emitted by clouds is usually almost unpolarized (Können 1985). If this unpolarized cloudlight is reflected from the horizontal glass surface of the water-dummies, it becomes partially polarized with always horizontal direction of polarization. Thus clouds can enhance the relative proportion of horizontally polarized reflected light in those regions of the reflector, from which nearly vertically polarized light would be reflected if the sky were clear. Since the percentage Q detected as water is predominantly governed by α of reflected light, the final consequence of clouds will be a slight increase of Q; the more extended the cloud cover, the larger is Q. This is clearly seen in Figs. 23.7 and 23.8. Thus, under a cloudy sky polarotactic water detection is slightly more efficient than under a clear sky with the same θ_S. Due to the frequent or durable occlusion of the

sun, under cloudy sky conditions the air temperature is usually lower than under clear sunny skies, which is advantageous for small-bodied flying aquatic insects, though the risk of predation is higher than at dusk. From this one can conclude that beside the sunset, the second most optimal period for polarotactic water seeking are the periods when the daytime sky is partly or totally cloudy.

For $\theta_S > 30^o$ the $Q(\theta_S)$ curve increases with θ_S in the case of the black water-dummy (Figs. 23.7 and 23.8). Therefore, at high θ_S Q of black waters could be as great as that at $\theta_S \approx 0^o$. This means that at high θ_S the polarimetric detection of dark waters can be as efficient or even more efficient than at sunset. However, when θ_S is high (near noon), the air temperature can be much higher, the air humidity much lower and the wind speed much greater than at dusk, which conditions are disadvantageous to small-bodied insects. Consequently, only certain large-bodied water-seeking polarotactic insects could take advantage of the large Q of dark waters at high θ_S. This may be the reason why have been such insects attracted to horizontal black plastic sheets not only at dusk, but also at noon (Bernáth et al. 2001b).

The shadows and mirror images influence only slightly the α-pattern of reflected skylight, especially for the black water-dummy (column 3 in Figs. 23.3 and 23.4). On the other hand, the p-pattern is strongly affected by these disturbances. Similar effect was observed by Pomozi et al. (2001b), who showed that the clear-sky α-pattern continues underneath many clouds. This phenomenon is of great biological importance, because the stability of the α-pattern against optical disturbances explains why the orientation of polarization-sensitive insects is governed predominantly by the α-pattern rather than the p-pattern: many terrestrial insects orient by means of the E-vector pattern of skylight (e.g. Wehner 1976) and water insects find their aquatic habitat by means of the horizontal polarization of reflected light (Schwind 1991).

Finally, the question arises, how the light reflected from the back surface of the glass pane of the water-dummies influenced the measured reflection-polarizational characteristics. Figure 23.10 shows the change of the intensity I of totally horizontally ($\perp$) or vertically ($||$) polarized light reflected from the front (I_1) or back (I_2) surface of a glass pane versus the angle of incident γ. Since $I_1^{\perp} \approx I_2^{\perp}$ for $\gamma < 55^o$ and $I_1^{||} \approx I_2^{||}$ for $\gamma < 75^o$, the back-reflection has practically no influence on the net polarization of reflected light for smaller angles of incidence (it only increases the net intensity by a factor of about 2). On the other hand, $I_1^{\perp} >> I_2^{\perp}$ for $\gamma > 65^o$ and $I_1^{||} >> I_2^{||}$ for $\gamma > 80^o$. Hence the intensity of back-reflection is negligible relative to that of the front reflection for larger angles of incidence, therefore the influence of back-reflection on the net polarization of reflected light is also negligible. Furthermore, Horváth and Pomozi (1997) calculated the polarizing characteristics of different reflectors composed of glass panes underlain by a metal mirror or various grey substrata. Their results also support that the back-reflection from the second glass surface affects only slightly the net polarization of reflected light. The patterns in Fig. 23.4 measured at the black water-dummy with back-reflection from the second glass surface are practically the same as those in Fig. 23.5 calculated for a perfectly black water without back-

reflection from a second surface. Gál et al. (2001a) measured the reflection-polarization patterns of the flat water surface under a clear sky at sunset. Comparing these patterns of a real dark water surface with the measured pattern of the black water-dummy, we can establish that they are practically the same. All these support that the back-reflection from the second surface of the glass affects only slightly the measurement of polarization.

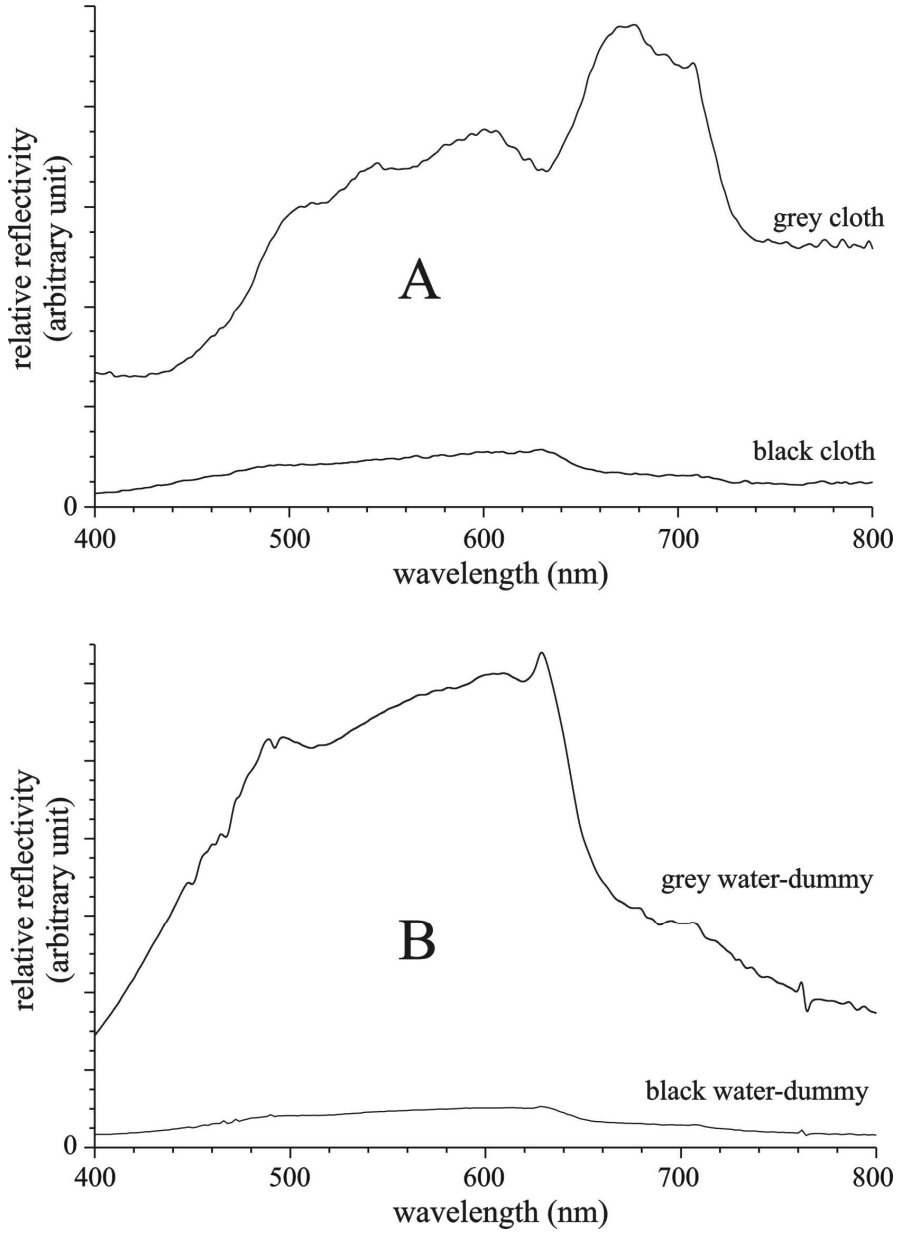

Fig. 23.1. (A) Relative reflectivity of the matt black and grey cloths used as substrata of the glass panes in the water-dummies. (B) Relative reflectivity of the black and grey water-dummies. (After Fig. 1 of Bernáth et al. 2003).

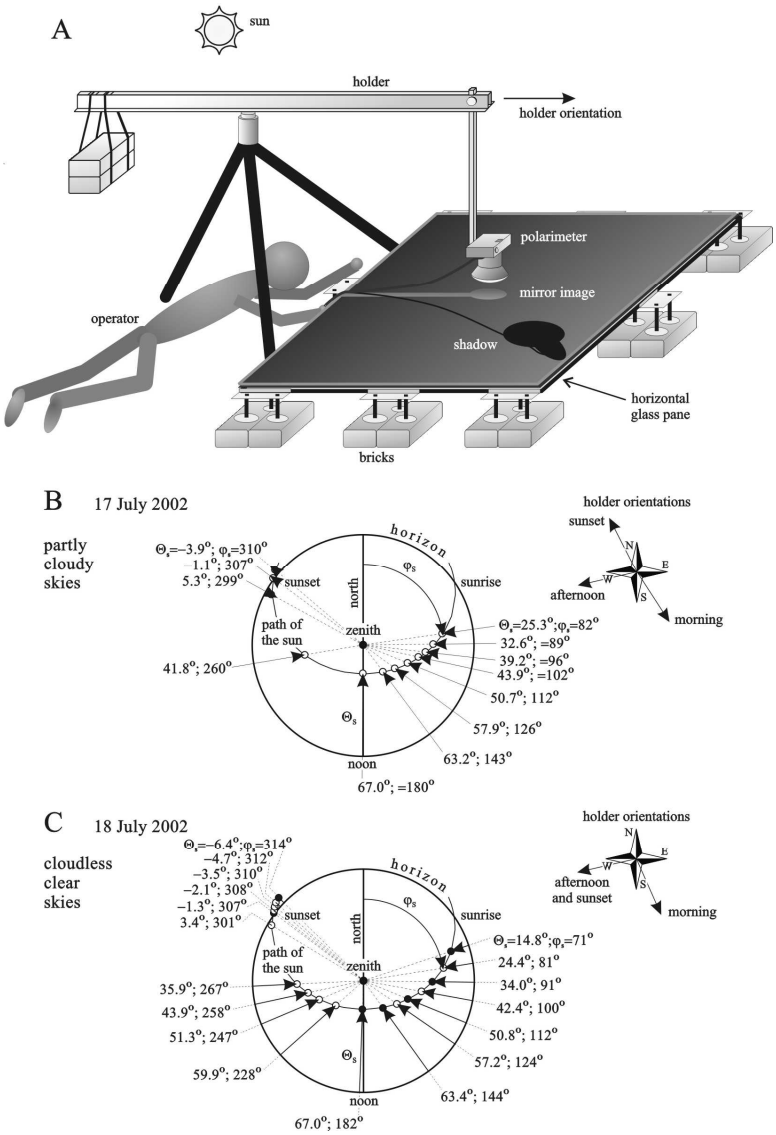

Fig. 23.2. (A) Experimental arrangement of the measurement of the reflection-polarizational characteristics of horizontal water-dummies. (B, C) The apparent celestial path of the sun during the measurements on 17 (partly cloudy skies) and 18 (clear, cloudless skies) July 2002 at the Hungarian Kunfehértó (46°23'N, 19°24'E) in a system of polar coordinates, where the solar azimuth angle φ_S is measured clockwise from the magnetic north, and the solar elevation θ_S is measured radially from the horizon. Dots show the solar positions when the measurements were performed. Black dots represent the solar positions when the patterns in Figs. 23.3 and 23.4 were measured. (After Fig. 2 of Bernáth et al. 2003).

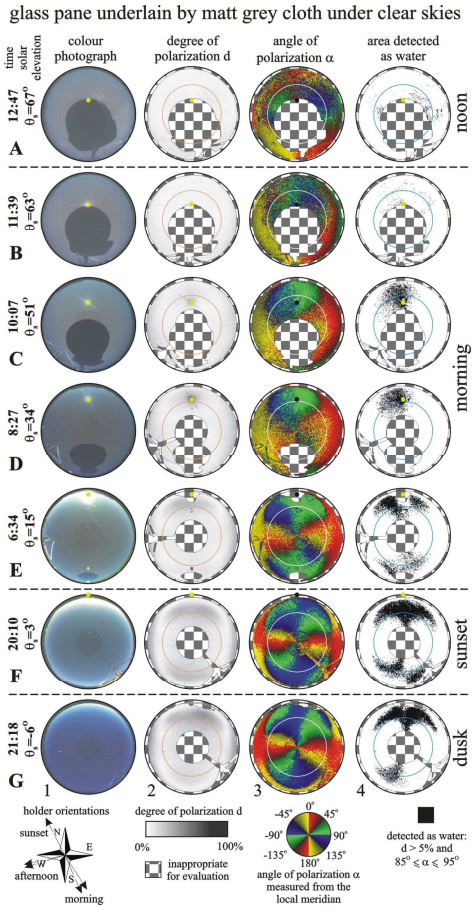

Fig. 23.3. Colour photographs (without polarizers) of the mirror image of the clear sky reflected from the grey water-dummy, patterns of the degree p and angle α (measured from the local meridian) of linear polarization of reflected skylight, and the area detected polarotactically as water as a function of the solar elevation θ_S. The grey water-dummy is composed of a horizontal glass pane underlain by a matt grey cloth, the reflection characteristics of which is shown in Fig. 23.1. The polarization patterns are measured by 180° field-of-view imaging polarimetry in the blue (450 nm). Chequered areas show those regions of the pictures, which are inappropriate for comparative analysis due to unwanted overexposure, shadows and mirror images of the polarimeter, its holder and remote cord. In column 4, regions are shaded by black, where $p > p_{tr} = 5\%$ and $85^\circ \le \alpha \le 95^\circ$. An imaginary polarotactic water insect is assumed to consider a surface as water if these two conditions are satisfied for the partially linearly polarized reflected light. In column 4 the regions where these criteria are not satisfied remained blank. The positions of the mirror image of the sun are shown by dots, the Brewster angle (56° from the nadir for glass with index of refraction $n_g = 1.5$) is represented by an inner circle within the circular patterns. Because of disturbing early morning dewfall, reflection-polarization patterns at low solar elevations are presented here only for the sunset and dusk period. (After Fig. 3 of Bernáth et al. 2003).

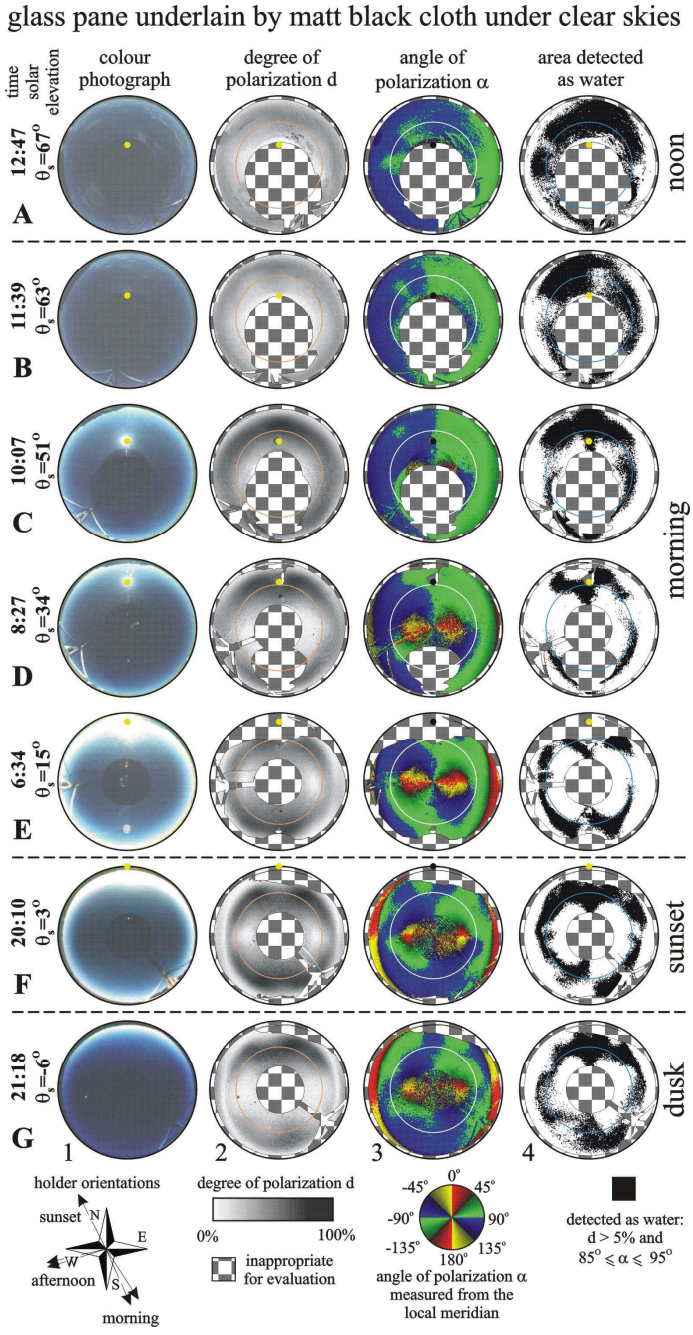

Fig. 23.4. As Fig. 23.3 for the black water-dummy composed of a horizontal glass pane underlain by a matt black cloth. (After Fig. 4 of Bernáth et al. 2003).

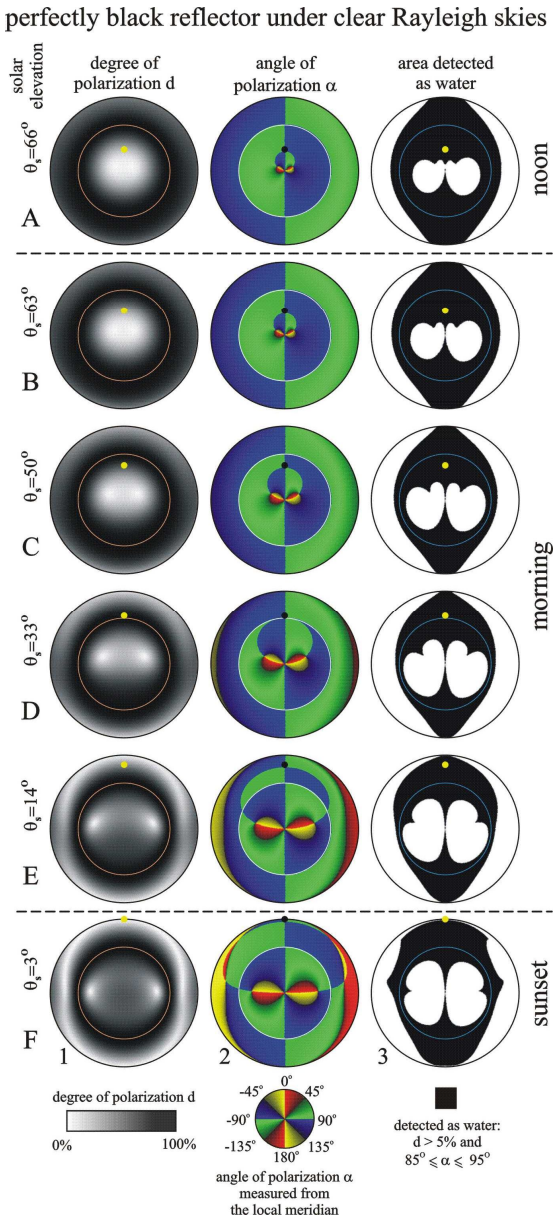

Fig. 23.5. As Fig. 23.3 (without colour photographs) for a perfectly black glass (with an index of refraction n_g = 1.5) reflector absorbing all penetrating light. Here the patterns of the degree p and angle α of linear polarization of reflected skylight are not measured, but they are calculated for incident single-scattered Rayleigh skylight with the use of the Fresnel formulae. The Brewster angle 56° (from the nadir for glass) is represented by a circle within the circular patterns. (After Fig. 5 of Bernáth et al. 2003).

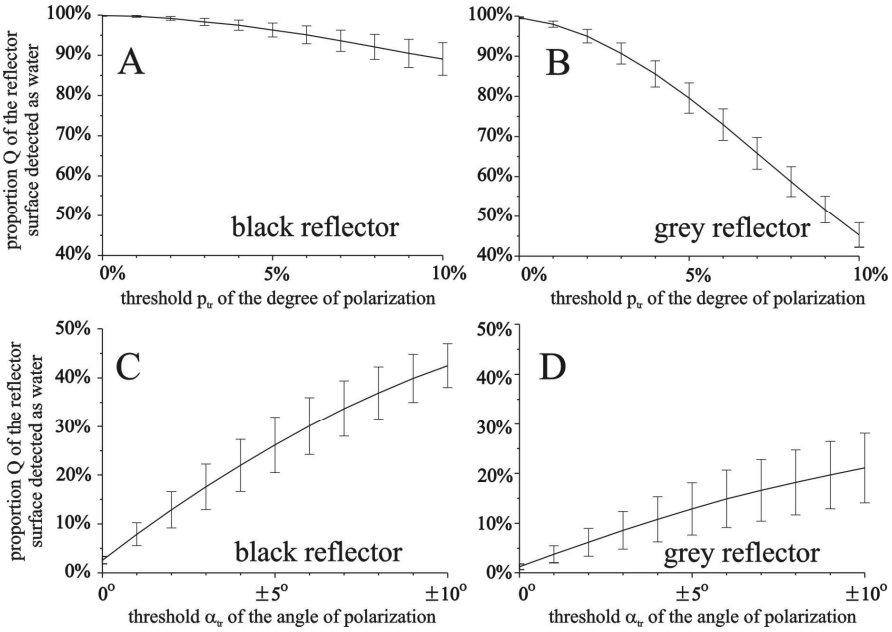

Fig. 23.6. Percentage Q of the whole lower hemispherical field of view (of an imaginary polarotactic water insect) in which the black (A, C) and grey (B, D) water-dummies are detected as water versus p_{tr} and $\Delta\alpha_{tr}$. It is assumed that the insect takes those regions of the dummies for water, from which partially linearly polarized light is reflected with degrees of linear polarization $p > p_{tr}$ or with angles of polarization α for which $|\alpha - 90^{\circ}| < \Delta\alpha_{tr}$, where α is measured from the local meridian. Q was calculated for the p- and α-patterns of the water-dummies measured in the blue (450 nm) and shown in Figs. 23.3 and 23.4. Q gives the proportion of the black areas in column 4 of Figs. 23.3 and 23.4 relative to the entire area of the region appropriate for comparative analysis (non-chequered regions in Figs. 23.3 and 23.4). Vertical bars show the intervals in which Q changed during the day from zero to the maximum (67°) solar elevation at given values of p_{tr} and $\Delta\alpha_{tr}$. The continuous curves are fitted to the centres of these vertical bars by the method of least squares. (After Fig. 6 of Bernáth et al. 2003).

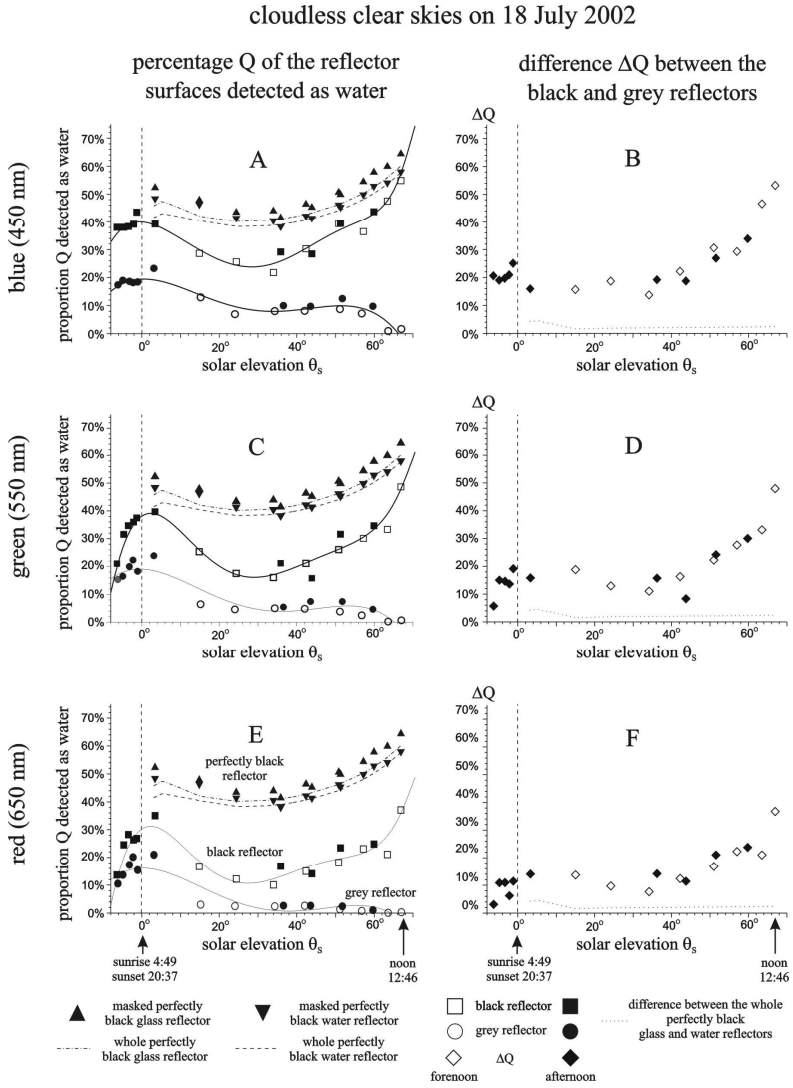

Fig. 23.7. Percentage Q detected as water for the black (squares) and grey (dots) water-dummies (A, C, E) and difference ΔQ between the black and grey water-dummies (rhombi) (B, D, F) as a function of the solar elevation θ_S in the blue (450 nm), green (550 nm) and red (650 nm). Data points measured forenoon and afternoon are symbolized by empty and filled squares/dots, respectively. The continuous curves are fitted to these data points by the method of least squares. The dashed/dashed-dotted $Q(\theta_S)$ curves are computed for the full area of a perfectly black glass (index of refraction $n_g = 1.5$) and water ($n_w = 1.33$) reflector absorbing all penetrating light. Triangles show the Q-values calculated for the perfectly black glass and water reflectors within the masked regions of the field of view appropriate for comparative analysis (non-chequered regions in the p- and α-patterns of Figs. 23.3 and 23.4). (After Fig. 7 of Bernáth et al. 2003).

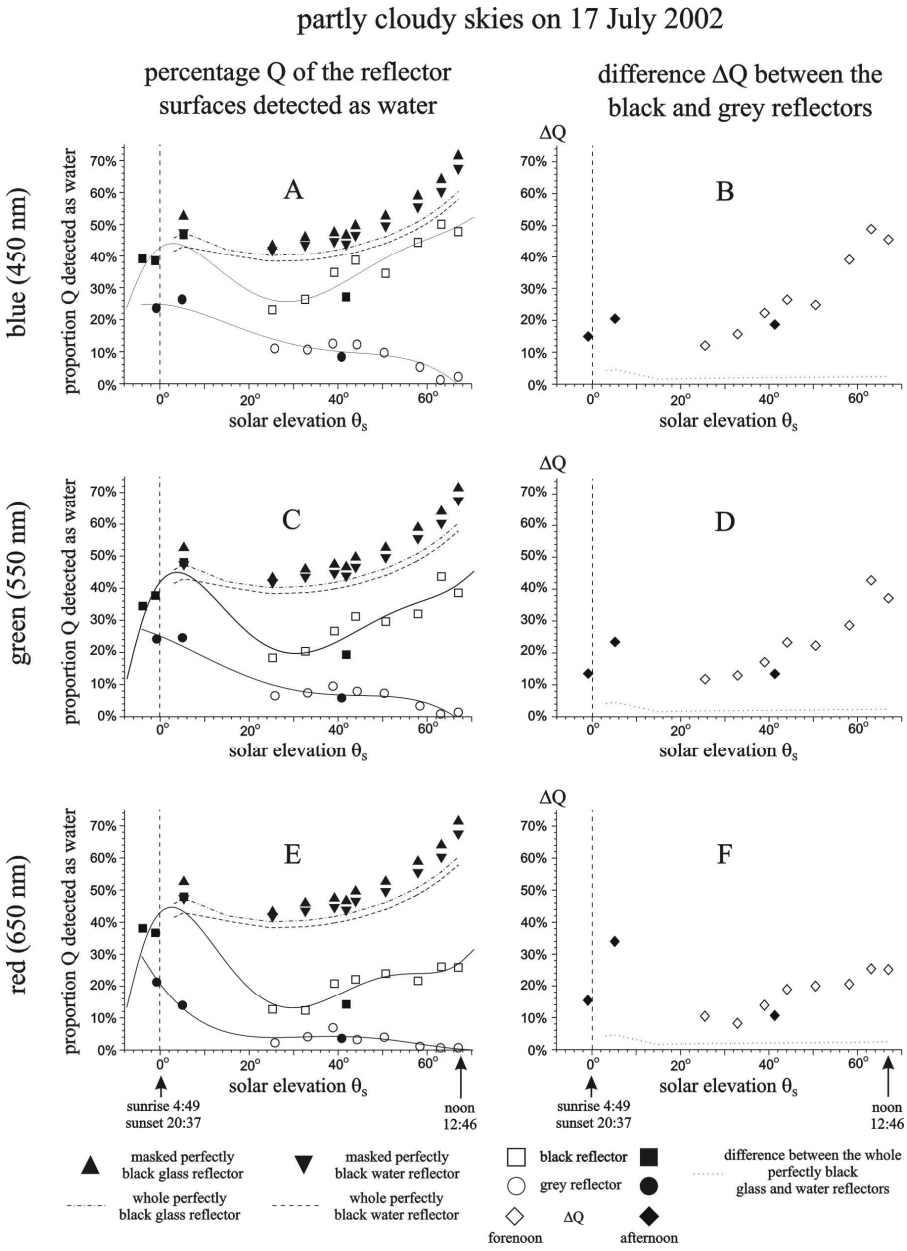

Fig. 23.8. As Fig 23.7 for partly cloudy skies on 18 July 2002. (After Fig. 8 of Bernáth et al. 2003).

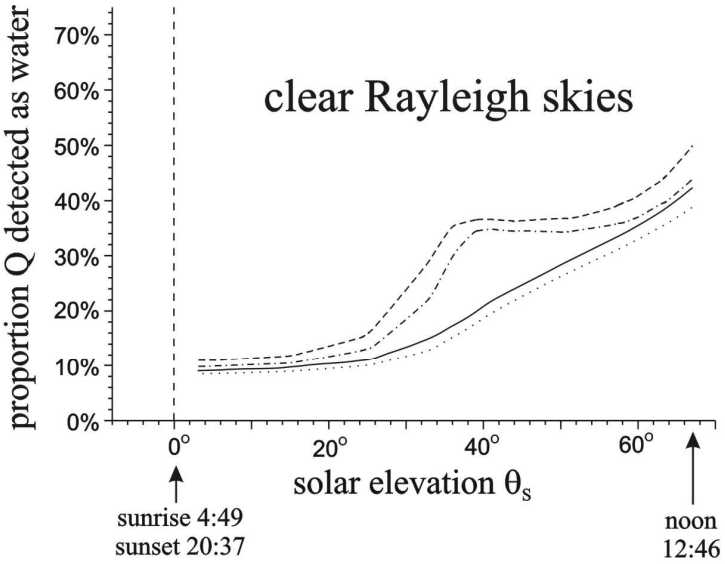

Fig. 23.9. As the left column in Fig. 23.7 calculated for the circular field of view within the nadir angle 35° and for the annular field of view between nadir angles 32° and 35° (representing the field of view of the polarization-sensitive ventral eye region of the backswimmer *Notonecta glauca*) of the patterns in column 3 of Fig. 23.5. (After Fig. 9 of Bernáth et al. 2003).

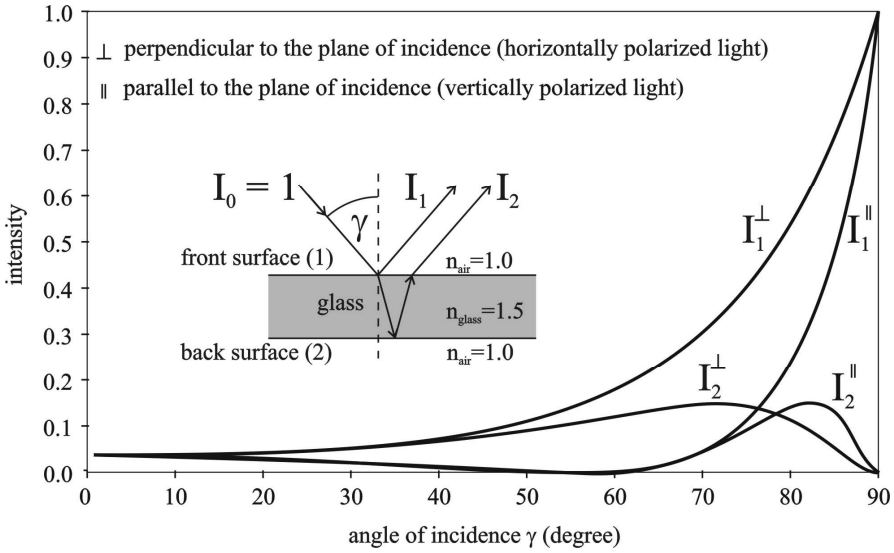

Fig. 23.10. Change of the intensity I of totally (with degree of linear polarization d = 100%) horizontally (⊥) or vertically (||) polarized light reflected from the front (1) or back (2) surface of a glass pane versus the angle of incident γ measured from the normal of the surface calculated with the use of the Fresnel formulae (Guenther, 1990), when the intensity of incident light is I_0 = 1. (After Fig. 10 of Bernáth et al. 2003).